Extending the Navier–Stokes solutions to transition regime in two-dimensional micro- and nanochannel flows using information preservation scheme

Ehsan Roohi and Masoud Darbandi[a)]
Department of Aerospace Engineering, Sharif University of Technology, P.O. Box 11365-8639, Tehran, Iran

(Received 15 January 2009; accepted 28 May 2009; published online 5 August 2009)

The kinetic-theory-based numerical schemes, such as direct simulation Monte Carlo (DSMC) and information preservation (IP), can be readily used to solve transition flow regimes. However, their high computational cost still promotes the researchers to extend the Navier–Stokes (NS) equations beyond the slip flow and to the transition regime applications. Evidently, a suitable extension would accurately predict both the local velocity profiles and the mass flow rate magnitude as well as the streamwise pressure distribution. The second-order slip velocity model derived from kinetic theory can provide relatively accurate velocity profiles up to a Knudsen (Kn) number of around 0.5; however, its mass flow rate accuracy decreases as Knudsen number approaches the upper bound. One remedy is to consider the rarefaction effects in calculating the NS viscosity coefficient. In this work, we use the shear stress distribution derived from our IP simulations, extend an analytical expression for the viscosity coefficient, impose it in the NS equations, and evaluate it via solving the transition regime. Using the new viscosity coefficient, we also derive an analytical expression for the mass flow rate, which provides accurate solutions for $\mathrm{Kn}<0.5$ and even beyond in micro- and nanochannel flows. We also show that the obtained streamwise pressure distribution agrees well with that of the DSMC-IP in this range. The current study is concerned with low speed diatomic gas flow through two-dimensional micro- and nanochannels. © *2009 American Institute of Physics*.
[DOI: 10.1063/1.3177351]

I. INTRODUCTION

Demands in design and fabrication of micro- and nanoelectromechanical systems have increased the need for better understanding of fluid flow and heat transfer behaviors at the micro- and nanoscales. The interaction of rarefaction and compressibility strongly affects the resulting flow behavior in such systems. There is also a wide range of heat and flow applications in micro- and nanoscale systems. They may work in a variety of flow regimes including continuum, slip, transition, and free molecular.[1] The Knudsen number is the key parameter to categorize the gas flow rarefaction. It is defined as the ratio of mean free path of the gas molecules to a characteristic dimension such as the channel height ($\mathrm{Kn}=\lambda/H$). If the Knudsen number is sufficiently small, i.e., $\mathrm{Kn}<0.01$, the fluid flow can be assumed as continuum and the Navier–Stokes (NS) equations can be used to analyze the flow while applying no-slip boundary conditions. The flow is then considered to be in slip regime for $0.01<\mathrm{Kn}<0.1$. In the slip regime, nonequilibrium effects dominate near the walls. However, the flow can still be analyzed by solving the NS equations and applying slip velocity and temperature jump boundary conditions. In the transition regime, $0.1<\mathrm{Kn}<10$, continuum-based equations fail to produce reliable solutions because rarefaction effects dominate and the thermodynamic equilibrium assumption starts breaking down. For $\mathrm{Kn}>10$, the flow is considered to be in free molecular regime. In this regime, intermolecular collisions are negligible comparing with the collisions between the gas molecules and the wall surfaces.

It is well known that molecular-based approaches, such as direct simulation Monte Carlo[2] (DSMC) and information preservation (IP) schemes[3] can be readily utilized to solve the flow field over the entire transition regime. However, their high computational costs have promoted the researchers to extend the NS equations beyond the slip flow regime and into the transition regime treatment. In past work, a variety of high-order slip velocity boundary conditions have been suggested to extend the NS solutions to higher rarefied gas flow treatments. However, they also show that the employment of high-order boundary conditions may not guarantee the accuracy of both velocity profiles and mass flow rate.[4] Karniadakis *et al.*[4] and Barber and Emerson[5] provided inclusive reviews of the slip boundary condition choices. One of the most accurate second-order slip boundary conditions, which is derived from the kinetic theory assumptions, is given by[4]

$$u_s=[u_\lambda+(1-\sigma_v)u_\lambda+\sigma_v u_w]/2, \tag{1}$$

where u is the streamwise velocity, the subscripts s and w stand for slip and wall, σ_v is the momentum accommodation factor, and λ indicates quantities evaluated at the edge of the Knudsen layer; a nonequilibrium region which extends up to a few (one to two) mean free paths away from the wall. This boundary condition predicts accurate wall slip velocity for

[a)]Author to whom correspondence should be addressed. Telephone: +98 (21) 6616-4944. Fax: +98 (21) 6602-2731. Electronic mail: darbandi@sharif.edu.

$\mathrm{Kn}<0.5$, although resulting in poor mass flow rate prediction.[4] There has been significant effort to improve the mass flow rate predictions; however, any expression with more accurate mass flow rate prediction has normally degraded the velocity profile prediction. For example, Aubert and Colin[6] suggested the second-order slip velocity as follows:

$$u_s - u_w = C_1 \ \mathrm{Kn}\frac{\partial u}{\partial y} + C_2 \ \mathrm{Kn}^2\frac{\partial^2 u}{\partial y^2}, \tag{2}$$

where $C_1=(2-\sigma_v)/\sigma_v$ and $C_2=9/8$. However, this slip velocity is biased toward predicting an accurate mass flow rate.[6] Beskok and Karniadakis[7] also suggested a unified slip velocity model for the entire Knudsen number regime as follows:

$$u_s - u_w = \frac{2-\sigma_v}{\sigma_v}\frac{\mathrm{Kn}}{1-b \ \mathrm{Kn}}\left(\frac{\partial u}{\partial y}\right), \tag{3}$$

where $b=-1$ is an arbitrary constant obtained from DSMC simulations. Although this model predicts accurate velocity profile for a wide range of Knudsen numbers, its mass flow rate prediction is still erroneous.

The high-order slip boundary conditions, e.g., Eqs. (1)–(3), have been widely applied to solve the NS equations for micro- to nanoflows at high Knudsen numbers. Aubert and Colin[6] applied Eq. (2) and solved the NS equations for accurate prediction of the mass flow rate in microchannels. Their results were in good agreement with the experimental data up to $\mathrm{Kn}_{\mathrm{out}}<0.25$.[8] Darbandi and co-worker[9,11] extended a compressible-incompressible pressure-based algorithm[12–14] to simulate micro- to nanoflows in the transition regime through short and long micro- and nanochannels. They employed the slip velocity boundary condition given by Eq. (1) and obtained accurate velocity profiles. Dongari *et al.*[15] used the second-order slip boundary condition, given by Eq. (2), with appropriate values for the first- and second-order slip coefficients in different Knudsen number regimes to calculate correct volume flow rate in the transition regime. In another attempt, Dongari *et al.*[16] modified the NS equations to include the diffusion of mass due to density and temperature gradients. They obtained accurate mass flow rate prediction in transition and free molecular flow regimes without using the concept of slip boundary condition. Zhang *et al.*[17] employed the homotopy analysis method and used the first- and second-order boundary conditions to find an accurate analytical solution for the NS equations. They achieved reliable results in the slip flow regime, however, with incorrect velocity profile predictions in the transition regime.

Generally, the NS equations derived on the basis of the Stokes assumption cannot be valid in the transition regime. One idea is to extend the stress-strain relation through the inclusion of a few higher-order terms into the primitive linear form. This normally results in more complicated relations between the stress and strain. Alternatively, another idea is to account for the rarefaction effects by modifying the viscosity coefficient as a function of Knudsen number, and to calculate the primitive shear stress relation. When using this technique, one essential task is to find the correct variation of viscosity coefficient with Knudsen number. Based on the simple analytical relations given for the viscosity coefficient at the two limits of continuum and free molecular regimes, Karniadakis *et al.*[4] considered the rarefaction effects and proposed a hybrid formula for the viscosity coefficient μ as follows:

$$\frac{\mu(\mathrm{Kn})}{\mu_0} = \frac{1}{1+\alpha \ \mathrm{Kn}} \tag{4}$$

where α is a coefficient and the subscript 0 denotes the value at the continuum extreme. To simulate the mass flow rate correctly, the coefficient α should be adjusted, for example, by using DSMC solution data. However, as is explained in Ref. 4, the simple relation given by Eq. (4) requires a complicated inverse hyperbolic-tangent function for α. To avoid such complexity, a mean value $\bar{\alpha}$ is usually employed. Karniadakis *et al.*[4] combined the above viscosity correction with their accurate unified slip velocity model, Eq. (3), and enhanced the accuracy of NS equations for the mass flow rate prediction.

A careful literature survey shows that the attempts for extending and solving the NS equations are mostly limited to obtaining either an accurate velocity profile[9–11,18–21] or a correct mass flow rate.[1,6,15,16] The main objective of the current work is to extend the accuracy of the NS equations beyond the slip regime and into the transition flow regime through micro- and nanochannels, where the velocity profile, the mass flow rate, and the streamwise pressure distribution should all be predicted correctly. We use the IP simulation data and suggest an analytical expression for the viscosity coefficient in terms of Knudsen number. The correlated viscosity coefficient is then combined with the second-order slip velocity boundary condition, Eq. (1), to derive analytical expressions for the mass flow rate magnitude and streamwise pressure distribution. To verify this technique, we extensively validate our derived analytical expressions against other available analytical and experimental data. The present work introduces a few contributions to micro- to nanoflow studies in the transition regime. First, although Karniadakis *et al.*[4] developed an expression to predict the viscosity coefficient for the entire transition regime, Eq. (4), there are major restrictions in choosing a suitable value for α. Therefore, Eq. (4) cannot be easily extended to arbitrary flow conditions without having sufficient information in advance about α. However, our viscosity coefficient expression does not include such a complicated parameter. Second, although the current viscosity coefficient expression is obtained via using the IP simulation data, it is very close to the experimentally confirmed viscosity model, which we derive from the velocity slip relation of Ref. 6. In other words, the current viscosity coefficient expression simulates the physical behavior of the flow field correctly. Third, Karniadakis *et al.*[4] used the DSMC mass flow rate to derive their analytical viscosity expression. This procedure requires significant numerical effort. Additionally, the DSMC data are quite noisy. Alternatively, we use a low scatter IP shear stress to obtain the variation of viscosity coefficient in terms of Knudsen num-

ber. This approach greatly reduces the preliminary computational costs. At the same time, we show that IP solutions for mass flow rate, shear stress, velocity, and streamwise pressure distribution are at the same level of accuracy as DSMCs. Finally, the new viscosity coefficient model predicts the mass flow rate and streamwise pressure distribution precisely if it is suitably combined with the second-order kinetic-based slip boundary condition given by Eq. (1). Comparisons of the current results with different experimental data demonstrate that the developed analytical mass flow rate relation is quite accurate in the early transition regime, $0.1 < \mathrm{Kn} < 0.5$.

The rest of this paper is organized as follows. Section II introduces and validates our developed IP scheme and describes the derivation of viscosity coefficient from the IP solution. Using the extended viscosity coefficient expression, we derive analytical expressions for the volume/mass flow rate and axial pressure and validate them in Sec. III. The concluding remarks are provided in Sec. IV.

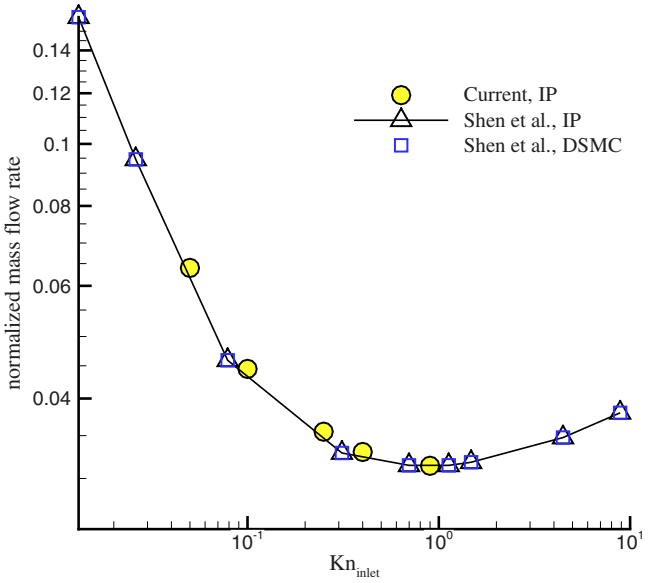

FIG. 1. (Color online) The current normalized IP mass flow rate in terms of inlet Knudsen number and comparison with those of Shen *et al.* (Ref. 30).

II. MODELING OF THE VISCOSITY COEFFICIENT

In this section, we describe and validate the DSMC-IP method. We then derive our IP-based viscosity coefficient expression and compare it with other available analytical expressions. Finally, IP velocity profiles are compared to different analytical and numerical solutions.

A. The DSMC-IP scheme

It is widely accepted that the DSMC is an accurate numerical tool to model the rarefied gas flows. In fact, DSMC simulates particle behavior in a manner consistent with what is described by the Boltzmann equation. The Boltzmann equation is the general governing equation for dilute gas flows. Consequently, the results of DSMC can be as accurate as the solutions of the Boltzmann equation, although providing that the cell size, time step, inlet/outlet boundary conditions, intermolecular and molecular-wall collision models, and so on are realistic. Although DSMC is a successful approach for simulating subsonic microflows,[22–26] its inherent statistical scatter does not allow it to be an efficient tool for the simulation of low speed gas flows. To remedy this deficiency, Fan and Shen[3] developed the IP scheme. IP scheme reduces the statistical scattering via preserving macroscopic flow information in the particles and the computational cells simulated in DSMC. In the IP scheme, the preserved macroscopic information is initially solved in a manner similar to that of the DSMC for the microscopic information. Then, it is modified to include the pressure force, which is the main driving force in most low speed flows. In fact, the IP scheme directly implements the pressure gradients on the preserved velocity field. This is contrary to the conventional DSMC, which implements pressure only at the inlet/outlet boundaries, and consequently, requires a longer time to influence the entire solution field. Consequently, the IP scheme greatly reduces the computational time compared to conventional DSMC simulations.[27,28] Sun and Boyd[29] further extended the IP scheme to simulate general subsonic microflows. They presented proper models for thermal energy fluxes and modified the basic molecular collision model. More details on the IP scheme can be found in Refs. 30 and 31.

B. IP validation

The current IP simulations are carried out for the nitrogen flow through a microchannel with a length to height ratio of $l/h=20$. We first provide important numerical parameters employed in our computations. The computational domain is discretized into 100×30 cells. The number of cells is selected after a careful grid study.[25] The cell sizes are $\Delta x_{\mathrm{cell}}=5.48\times 10^{-8}$ m$=2\lambda$ and $\Delta y_{\mathrm{cell}}=9.14\times 10^{-9}$ m$=\lambda/3$, where the mean free path is $\lambda=2.74\times 10^{-8}$ m. Each cell is subsequently divided into two subcells in each direction. Since the gradients of flow properties are relatively small in the streamwise direction, the cell size can be larger than mean free path in the x-direction.[27,30,32] We set 40–50 molecules in each cell at time zero. The time step is adjusted to be smaller than mean collision time and satisfy a Courant–Friedrichs–Lewy number, based on the most probable molecular speed V_{mp}, smaller than 1, i.e., $\Delta t=1\times 10^{-11}$ s. The values of the mass flow rate at the inlet and outlet are monitored until achieving negligible difference between the two consequent time steps. A sample size of 1.5×10^{5} is used to obtain a smooth IP solution.

Before deriving an analytical expression for the viscosity coefficient via IP, we wish to validate the IP mass flow rate. In this regard, we define the normalized mass flow rate as $\dot{m}^{*}=\dot{m}/(\rho_{\mathrm{avg}}\sqrt{2RTh/2})$, where ρ_{avg} is the average value of inlet and outlet densities, R is the universal gas constant, and T is temperature. Figure 1 shows the variation of normalized IP mass flow rate with inlet Knudsen number and compares it with IP and DSMC solutions of Shen *et al.*[30] The inlet/outlet pressure ratio is $\Pi=1.428$. As is observed, there is good agreement between the current solutions and those of Ref. 30.

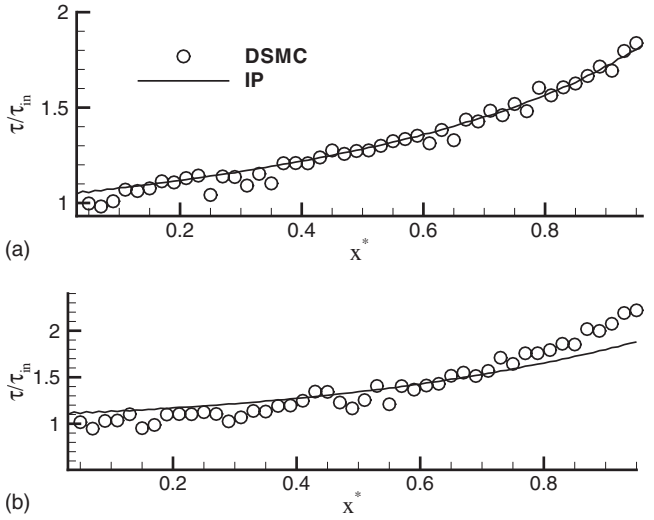

FIG. 2. DSMC and IP normalized wall shear stress distributions along the channel for different inlet/outlet Knudsen magnitudes. (a) $Kn_{in}=0.05$, $Kn_{out}=0.18$; (b)$Kn_{in}=0.1$, $Kn_{out}=0.3$.

The use of the IP technique to generate the modified viscosity used in the NS equations is the key assumption in this analysis. Without detailed proof that IP reproduces the shear stress predicted by DSMC under similar conditions, we are left to wonder whether the good agreement demonstrated for mass flow rate could be fortuitous. To expand our validation study, we also compare the IP wall shear stress distribution along the channel with that of DSMC. They are obtained from

$$\tau_{w,\mathrm{DSMC}}(x)=\left[F_{\mathrm{num}}\sum_{j=1}^{N_s}m(c_{t,j}^{\mathrm{in}}-c_{t,j}^{\mathrm{re}})\right]\Big/\,t_sA, \tag{5a}$$

$$\tau_{w,\mathrm{IP}}(x)=\left[\sum_{j=1}^{N_s}m(V_{t,j}^{\mathrm{in}}-V_{t,j}^{\mathrm{re}})\right]\Big/\,t_sA, \tag{5b}$$

where V is the particle information velocity, τ_w is the wall shear stress, c is the molecular velocity, F_{num} is the ratio of the real to simulated molecules, N_s is the total number of molecules colliding the wall element during the period of t_s, A is the area of the wall element, and m is the molecular mass. The subscript t denotes tangential and the superscripts in and re denote the values before and after colliding with the wall, respectively. Figure 2 shows the distribution of the DSMC and IP normalized wall shear stress solutions along the channel at different inlet/outlet conditions. In this figure, the shear stress is normalized with its inlet value. Similar to the results given in Refs. 27 and 29, this figure shows that both IP and DSMC predict almost identical shear stress distributions; however, the IP solution has much less statistical scattering. This is the key reason why we choose IP rather than the conventional DSMC to derive analytical expression for the viscosity coefficient. As is shown in Refs. 27 and 30 (and also in the next sections), IP scheme can be considered as accurate as DSMC; however, IP provides smoother solutions for velocity, shear stress, and pressure distribution in low speed channel flows while it needs lower computational cost.

It should be recalled that the IP collision model is the determining factor for the accuracy of shear stress calculation. The preliminary IP collision model of Refs. 27 and 28 assumes that the preserved information of particles is the same after collision; while the numerical tests[29] show that this basic model cannot correctly simulate the viscosity and thermal conductivity of gas flows. Sun and Boyd[29] suggested a phenomenological model for the distribution of the information after collision based on the collision deflection angle. Comparing with theory and DSMC solutions, their model accurately predicts shear stress distribution in the Couette flow. In Sec. II E, we use both of these collision models and evaluate their impacts on the accuracy of the IP solutions. To distinguish them from each other, we name the preliminary and phenomenological collision models as collision models 1 and 2, respectively.

C. IP shear stress and viscosity coefficient calculations

After validating the current IP wall shear stress, we may use it to derive an expression for the viscosity coefficient as a function of Knudsen number, μ (Kn). That is,

$$\mu_e(\mathrm{Kn})=\frac{\tau_{w,\mathrm{IP}}(x)}{\partial V_t/\partial n}, \tag{6}$$

where μ_e is the effective viscosity. Although a linear relation between stress and strain would suffice to describe their dependency in low Knudsen numbers, a nonlinear relation between them should be considered in higher Knudsen numbers. This can be achieved via imposing higher-order terms in wall shear stress calculations as follows:

$$\begin{aligned}\tau_{w,\mathrm{IP}}&=\tau_w^{(\mathrm{NS})}+\tau_w^{(\mathrm{B})}+\tau_w^{(\mathrm{AB})}+\cdots\\&=\mu_{\mathrm{NS}}\frac{\partial V_t}{\partial n}+\tau_w^{(\mathrm{B})}+\tau_w^{(\mathrm{AB})}+O(\mathrm{Kn}^4),\end{aligned} \tag{7}$$

where the superscripts NS, B, and AB denote the Navier–Stokes, the Burnett, and the augmented Burnett equations, respectively. However, we reduce this equation suitably to derive an effective viscosity coefficient for the NS equations in the early transition regime. In this regard, we suggest

$$\begin{aligned}\tau_{w,\mathrm{IP}}(x)&\approx\mu_{e,\mathrm{NS}}(x)\frac{\partial V_t}{\partial n}+\tau_w^{(\mathrm{B})}+O(\mathrm{Kn}^3)\\&\approx\mu_{e,\mathrm{NS}}(x)\frac{\partial V_t}{\partial n}+O(\mathrm{Kn}^3).\end{aligned} \tag{8}$$

It is because the value of $\tau_w^{(\mathrm{B})}$ is negligible for low Mach isothermal flows in long microchannels.[4] On the other hand, since our concern is to correct the mass flow rate of the NS equations rather than the AB equations, keeping other stress terms in Eq. (7), such as $\tau_w^{(\mathrm{AB})}$, may not be justified. Of course, the validity of Eq. (8) degrades as Knudsen number increases. Using Eq. (8) to calculate the viscosity coefficient, we can bridge between the IP shear stress and the NS viscosity coefficient, extend the NS applicability beyond the

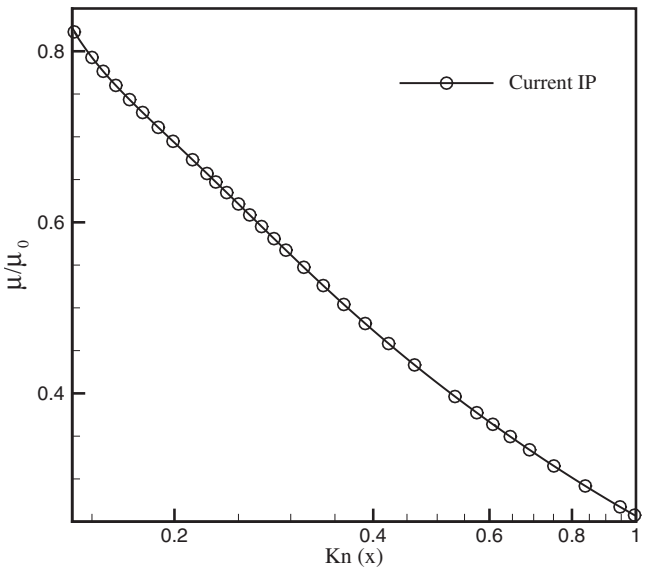

FIG. 3. Variation of the normalized IP-based viscosity coefficient with Knudsen number in a channel with early transition regime flow.

slip flow regime limit, and predict the mass flow rate magnitude more accurately.

Figure 3 shows the variation of the normalized viscosity coefficient obtained from Eq. (8) with Knudsen number in midtransition regime. The viscosity coefficient is normalized with its unmodified value μ_0, derived at $\mathrm{Kn}\to 0$. In performing IP simulations, we have considered full momentum accommodation factor at the walls, $\sigma_v=1$. We have carried out different independent runs in order to collect data. This figure shows that the viscosity coefficient decreases as Knudsen number increases. As was mentioned earlier, the validity of Eq. (8) would decrease as Knudsen number increases further. It is because the Knudsen layer grows in the channel and a linear approximation turns out to be invalid for higher Knudsen number values.[20] In this study, we concentrate on a range of $0.1<\mathrm{Kn}<0.5$, where the slip prediction given by Eq. (1) is accurate and likely there would be less errors in employing Eq. (8).

D. Derivation of the NS-based and IP-based viscosity coefficient expressions

Using the second-order slip boundary condition given by Eq. (1), the velocity profile in the flow field can be obtained from[4]

$$u(x,y)=\frac{h^2}{2\mu}\frac{dp}{dx}\left[\left(\frac{y}{h}\right)^2-\frac{y}{h}-\left(\frac{2-\sigma_v}{\sigma_v}\right)(\mathrm{Kn}-\mathrm{Kn}^2)\right], \quad (9)$$

where dp/dx is the pressure gradient along the channel. Imposing a general wall slip velocity boundary condition, i.e., Eq. (2), the mass flow rate $\dot{m}$ can be calculated from

$$\dot{m}=\int_0^h(\rho u)dy=\int_0^h\frac{h^2}{2\mu RT}pdp\Phi(y,\mathrm{Kn})dy, \quad (10)$$

where density is related to temperature via the equation of state, $\rho=p/(RT)$, and Φ is a general function, which depends on the imposed general slip velocity boundary condition. Assuming isothermal flow conditions and considering a one-dimensional axial pressure variation, the integral argument becomes only a function of Φ. The integration along the streamwise direction gives the total mass flow rate as follows:

$$\int_0^l\dot{m}dx=\dot{m}l=\int_{p_{\mathrm{in}}}^{p_{\mathrm{out}}}\frac{h^2}{2\mu RT}\left(\int_0^h\Phi(y,\mathrm{Kn})dy\right)pdp, \quad (11)$$

where p_{in} and p_{out} are the inlet and outlet pressures, respectively. We assume that the viscosity coefficient is a function of the Knudsen number, $\mu=\mu(\mathrm{Kn})$, and keep it in the integral argument. For isothermal flow, the Knudsen number is related to pressure via $\mathrm{Kn}_{\mathrm{out}}p_{\mathrm{out}}=\mathrm{Kn}(x)p$. As we described in Sec. I, the Aubert–Colin second-order velocity profile model, given by Eq. (2) with slip coefficients $C_1=(2-\sigma_v)/\sigma_v$ and $C_2=9/8$, predicts an accurate mass flow rate for $\mathrm{Kn}<0.25$. The mass flow rate corresponding to the Aubert and Colin model is obtained from[6]

$$\dot{m}=\frac{h^3p_{\mathrm{out}}^2}{24\mu_0RTl}\left[\Pi^2-1+12\left(\frac{2-\sigma_v}{\sigma_v}\right)(\Pi-1)\mathrm{Kn}_{\mathrm{out}}+27\ \mathrm{Kn}_{\mathrm{out}}^2\ln(\Pi)\right]. \quad (12)$$

If we substitute $\dot{m}$ from Eq. (12) in Eq. (11) and keep the viscosity as a function of Knudsen number, it yields

$$\frac{hp_{\mathrm{out}}^2}{12\mu_0}\left[\Pi^2-1+12\left(\frac{2-\sigma_v}{\sigma_v}\right)(\Pi-1)\mathrm{Kn}_{\mathrm{out}}+27\ \mathrm{Kn}_{\mathrm{out}}^2\ln(\Pi)\right]=\int_{p_{\mathrm{in}}}^{p_{\mathrm{out}}}\left\{\frac{1}{\mu(\mathrm{Kn})}\int_0^h\left[\frac{y}{h}-\left(\frac{y}{h}\right)^2+\left(\frac{2-\sigma_v}{\sigma_v}\right)(\mathrm{Kn}-\mathrm{Kn}^2)\right]dy\right\}pdp. \quad (13)$$

Taking the above integration, we eventually derive an expression for the viscosity coefficient as follows:

$$\left[\frac{\mu(\mathrm{Kn})}{\mu_o}\right]_{\mathrm{NS}}=\frac{\frac{\sigma_v}{2-\sigma_v}+6\ \mathrm{Kn}-6\ \mathrm{Kn}^2}{\frac{\sigma_v}{2-\sigma_v}+6\ \mathrm{Kn}+13.5\ \mathrm{Kn}^2}, \quad (14)$$

where the subscript NS refers to the fact that Eq. (14) is derived from the NS-based mass flow rate relation given by Eq. (12). Since Eq. (12) agrees well with experiment[8] for $\mathrm{Kn}<0.25$, it is expected that the resulting viscosity coefficient would be accurate enough for this range of Knudsen number as well. Equation (14) indicates that the viscosity varies quadratically with the Knudsen number. Considering Eq. (14), we similarly consider the IP-based viscosity

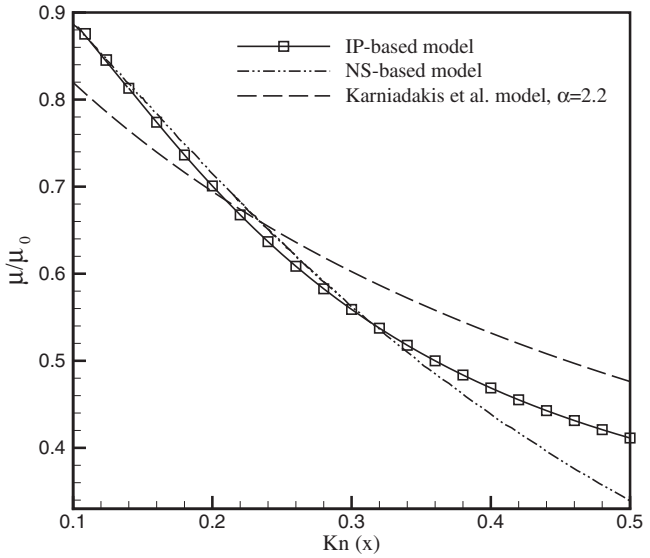

FIG. 4. Comparing the current IP-based and NS-based viscosity coefficient models with that of Karniadakis *et al.* (Ref. 4).

coefficient variation shown in Fig. 3, use regression, and derive a new quadratic expression for the viscosity coefficient, although for a wider range of Knudsen numbers, $0.1 < \mathrm{Kn} < 0.5$. The resulting expression is given by

$$\left[\frac{\mu(\mathrm{Kn})}{\mu_0}\right]_{\mathrm{IP}} = \frac{\frac{\sigma_v}{2-\sigma_v} + 0.89\ \mathrm{Kn} + 4.70\ \mathrm{Kn}^2}{\frac{\sigma_v}{2-\sigma_v} + 0.75\ \mathrm{Kn} + 19.98\ \mathrm{Kn}^2}, \tag{15}$$

where the subscript IP refers to the fact that it has been derived from the IP simulation data. We name it the IP-based viscosity coefficient model. Figure 4 presents the normalized viscosity coefficient given by Eq. (15), and compares it with the NS-based viscosity coefficient, Eq. (14), and the relation of Karniadakis *et al.*, Eq. (4), with an average value for α equal to 2.2. It should be noted that Karniadakis *et al.*[4] suggested $\alpha=2.2$ for the nitrogen flow in a channel with a pressure ratio of 2.28 and $\mathrm{Kn}_{\mathrm{out}}=0.2$. A few important conclusions can be derived from this figure. First, the NS-based viscosity coefficient is close to the current IP-based model as long as $\mathrm{Kn} \leq 0.3$. As previously stated, this is the valid range for Eq. (12). Second, the model of Karniadakis *et al.* with $\alpha=2.2$ only agrees with IP- and NS-based models around $\mathrm{Kn} \sim 0.2$. It is at this point that Ref. 4 suggests $\alpha=2.2$. Although the current IP-based viscosity coefficient model has been derived based on some specific conditions, i.e., $\Pi=2$, $\sigma_v=1$, and $\mathrm{Kn}_{\mathrm{out}}=0.2$, we will show that its validity is not restricted to these conditions and it performs suitably over wider ranges of pressure ratios, accommodation coefficients, and outlet Knudsen numbers (see Secs. III B and III C).

We should note that the viscosity coefficient is not the sole parameter in determining the mass flow rate. Indeed, its combination with the slip boundary condition (this combination is called *slip coefficient*) determines the mass flow rate. Due to the important role of velocity profile in accurate mass flow rate predictions, we first compare the velocity profiles derived from different slip boundary conditions with each other and then evaluate their resulting mass flow rates.

E. Velocity profiles

As was previously stated in Sec. II B, we have two options in the choice of collision models, collision model 1 (Ref. 3) or 2 (Ref. 29) to perform the IP simulation. We refer to the resulting velocity profiles as models 1 and 2, respectively. Figure 5 compares the current IP velocity profiles with DSMC results, the linearized Boltzmann (LB) solution of Ohwada *et al.*,[33] the second-order slip velocity model, Eq. (1), and the Beskok unified model,[7] Eq. (3). The results are provided for five Knudsen numbers. The velocity is normalized by its mean value ($U^*=U/U_{\mathrm{mean}}$) and the distance by the channel height ($y^*=y/h$). The figure collects valuable information about the accuracy of different numerical and analytical solutions. Following the descriptions provided in Sec. II A, the solution of DSMC can be considered as the closest one to that of the Boltzmann equation. Therefore, we consider DSMC as the most accurate solution and evaluate all other solutions against it. As can be seen, the LB solution underpredicts the slip velocity at all Knudsen numbers. The second-order kinetic model is accurate for both the slip and maximum velocity magnitudes in lower Knudsen numbers; however, its accuracy starts deteriorating from the centerline as the Knudsen number increases, see Fig. 5(c), and then this deterioration propagates into the entire flow region, see Fig. 5(d). Generally, the NS slip velocity models have been extended in a way to match the real velocity profile either at the wall and inside the Knudsen layer or at the center line and outside the Knudsen layer. The slip boundary condition given by Eq. (1) predicts a correct slip velocity magnitude at the wall for moderate Knudsen numbers. However, its implementation underpredicts the maximum velocity at the centerline. This is due to different characteristics of inner (Knudsen layer region) and outer (main flow region) layers.

Another key point in Fig. 5 is that there are slight inaccuracies in both slip velocity (overprediction) and maximum velocity (underprediction) for both of the current IP collision models when $\mathrm{Kn} < 0.667$. Cai *et al.*[27] similarly showed that the IP velocity prediction is not in full agreement with that of DSMC. The figure shows that both IP collision models demonstrate this discrepancy although collision model 2 performs slightly better. However, it should be recalled that the IP solution predicts mass flow rate and shear stress very close to that of DSMC. For low Knudsen numbers, the Beskok analytical model, Eq. (3), overpredicts the maximum velocity. As Knudsen number increases, it overpredicts the slip velocity; see Fig. 5(c), but it correctly predicts the maximum velocity.

As will be shown later, the combination of our IP-based viscosity coefficient model, Eq. (15), with the second-order

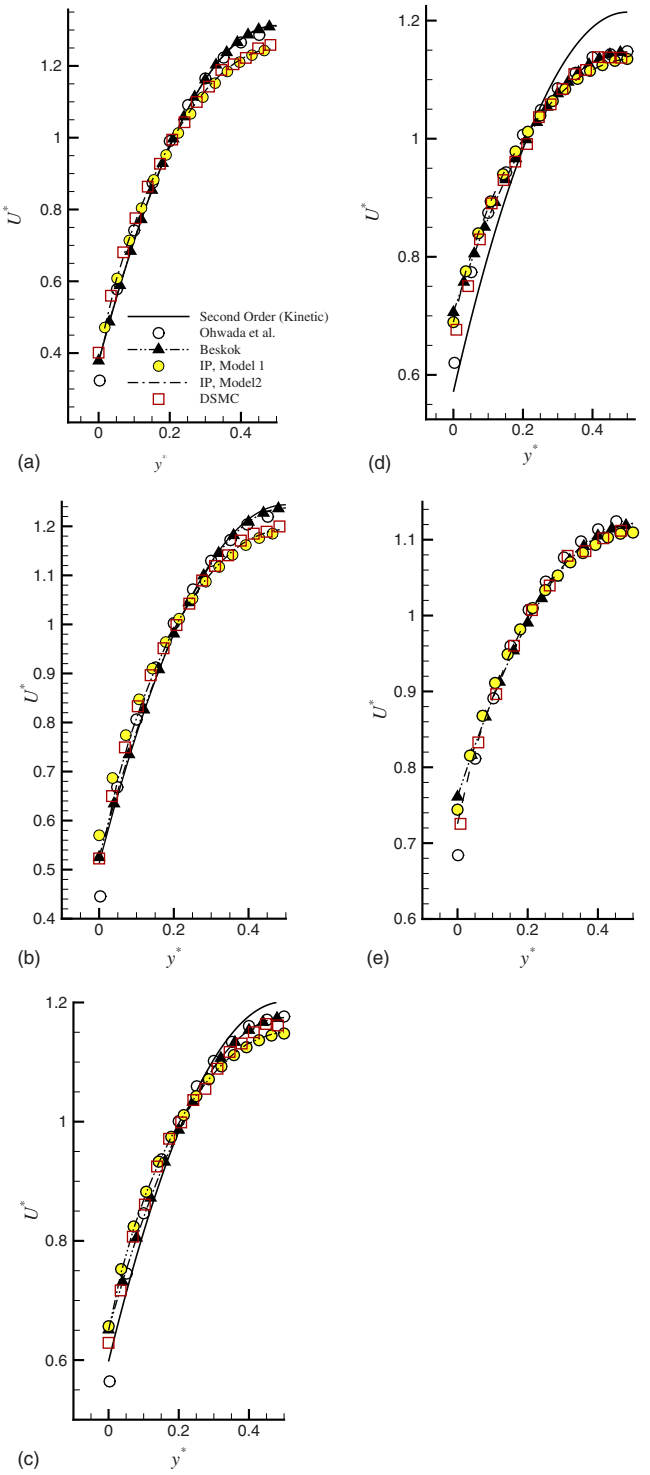

FIG. 5. (Color online) Comparing the current DSMC and IP (with two collision models 1 and 2) velocity profiles with those of LB of Ohwada *et al.* (Ref. 33), the NS solution of Beskok and Karniadakis (Ref. 7), and the second-order kinetic-theory-based relation, Eq. (9), at different Knudsen numbers. (a) Kn=0.113; (b) Kn=0.226; (c) Kn=0.451; (d) Kn=0.667; (e) Kn=1.13.

kinetic model, results in an accurate mass flow rate prediction for the early transition regime, Kn < 0.5. As is confirmed by the results in Fig. 5, the second-order kinetic model is relatively accurate within this Knudsen number range; therefore, our viscosity model is also physically accurate.

III. MASS FLOW RATE AND PRESSURE DISTRIBUTION STUDIES

In this section, we use our IP-based viscosity coefficient model, Eq. (15), and derive an analytical expression for the mass flow rate. We then investigate the accuracy of our expression against other analytical solutions considering different flow conditions. Finally, the axial pressure distribution is assessed.

A. Derivation of the IP-based slip coefficient

Using the current IP-based viscosity coefficient model, Eq. (15), we further incorporate it with the second-order slip velocity expression, Eq. (9), to calculate the volume/mass flow rate analytically. For a general slip boundary condition, the normalized volumetric flow rate can be derived from[4]

$$\frac{\dot{Q}}{\dot{Q}_c} = \frac{1}{\mu(\mathrm{Kn})}[1 + 6(C_1\ \mathrm{Kn} + C_2\ \mathrm{Kn}^2)], \tag{16}$$

where the subscript c denotes the continuum regime and C_1 and C_2 are the coefficients described in Eq. (2). Table I provides the values of C_1, C_2, and $\mu(\mathrm{Kn})$ for a few important slip velocity models including the first-order Maxwell,[4] the second-order kinetic-theory,[4] the current IP-based model, Karniadakis *et al.*,[4] Aubert and Colin,[6] and Hadjiconstantinou model.[34] Using the second-order kinetic-theory slip velocity and the IP-based viscosity coefficient model, Eq. (16) can be rewritten as

$$\frac{\dot{Q}}{\dot{Q}_c} = \frac{\dfrac{2-\sigma_v}{\sigma_v} + 0.75\ \mathrm{Kn} + 19.98\ \mathrm{Kn}^2}{\dfrac{2-\sigma_v}{\sigma_v} + 0.89\ \mathrm{Kn} + 4.70\ \mathrm{Kn}^2} \times \left[1 + 6\frac{2-\sigma_v}{\sigma_v}(\mathrm{Kn} - \mathrm{Kn}^2)\right]. \tag{17}$$

Assuming $\sigma_v = 1$, multiplying Eq. (17) by ρ, and integrating it along the axial direction, we can eventually derive an expression for the normalized mass flow rate, or rather the slip coefficient. It is given by

$$S_{\mathrm{IP}} = \frac{\dot{m}}{\dot{m}_c} = 1 + a_1\frac{\mathrm{Kn}_{\mathrm{out}}}{1+\Pi} + \frac{\mathrm{Kn}_{\mathrm{out}}^2}{1-\Pi^2} \times [51.00\ \ln(\Pi) + 34.07\ \ln(a_2)], \tag{18}$$

where a_1 and a_2 are defined as

$$a_1 = 11.72 + \frac{89.90 \times 0.47}{1 + \left(0.21 + \dfrac{0.47}{\mathrm{Kn}_{\mathrm{out}}}\right)\left(0.21 + \dfrac{0.47\Pi}{\mathrm{Kn}_{\mathrm{out}}}\right)}, \tag{19}$$

$$a_2 = \frac{1 + 0.89\ \mathrm{Kn}_{\mathrm{out}} + 4.70\ \mathrm{Kn}_{\mathrm{out}}^2}{\Pi^2 + 0.89\ \mathrm{Kn}_{\mathrm{out}}\Pi + 4.7\ \mathrm{Kn}_{\mathrm{out}}^2}.$$

It may be noted that the coefficients that appeared in the

TABLE I. The required coefficients for the normalized flow rate expression, see Eq. (16).

Model	C_1	C_2	$\mu(\mathrm{Kn})/\mu_0$
Maxwell,[a] first-order	$\frac{2-\sigma_v}{\sigma_v}$	0	1
Second-order kinetic theory[a]	$\frac{2-\sigma_v}{\sigma_v}$	$-\frac{2-\sigma_v}{\sigma_v}$	1
Current IP-based model	$\frac{2-\sigma_v}{\sigma_v}$	$-\frac{2-\sigma_v}{\sigma_v}$	$\frac{1+0.75\ \mathrm{Kn}+19.98\ \mathrm{Kn}^2}{1+0.89\ \mathrm{Kn}+4.70\ \mathrm{Kn}^2}$
Karniadakis *et al.*[a]	$\frac{2-\sigma_v}{\sigma_v}\frac{\mathrm{Kn}}{1-b\ \mathrm{Kn}}$	⋯	$\frac{1}{1+\alpha\ \mathrm{Kn}}$
Aubert and Colin,[b] second-order	$\frac{2-\sigma_v}{\sigma_v}$	$\frac{27}{12}$	1
Hadjiconstantinou[c] (modified Cercignani model)	1.11	0.62	1

[a]Reference 4.
[b]Reference 6.
[c]Reference 34.

IP-based viscosity coefficient model similarly reappear in the IP-based slip coefficient expression. For the general second-order boundary condition given by Eq. (2), the slip coefficient reduces to

$$S = 1 + 12C_1\frac{\mathrm{Kn}_{\mathrm{out}}}{\Pi+1} + 12C_2\frac{\mathrm{Kn}_{\mathrm{out}}^2}{\Pi^2-1}\ln(\Pi). \tag{20}$$

Although the above equation seems quite simple, it is derived from a slip velocity profile which is correct for either mass flow rate calculation or velocity profile prediction. In fact, it does not include any viscosity coefficient correction. If the viscosity correction is incorporated in this expression, we obtain a more comprehensive formula similar to Eq. (18). Considering this point, Karniadakis *et al.*[4] derived a relation for the slip coefficient using their unified velocity profile, Eq. (3), and their empirical relation for the viscosity coefficient, Eq. (4). Their attempts resulted in

$$S = \frac{\dot{m}}{\dot{m}_c} = \frac{\Delta p}{(\Pi^2-1)p_{\mathrm{out}}}\left[\Pi + 1 + 2\left(6\frac{2-\sigma_v}{\sigma_v}+\alpha\right)\mathrm{Kn}_{\mathrm{out}} + 12\frac{2-\sigma_v}{\sigma_v}\frac{b+\alpha}{\Pi-1}\mathrm{Kn}_{\mathrm{out}}^2\ln\left(\frac{\Pi-b\ \mathrm{Kn}_{\mathrm{out}}}{1-b\ \mathrm{Kn}_{\mathrm{out}}}\right)\right], \tag{21}$$

where $\Delta p = p_{\mathrm{in}} - p_{\mathrm{out}}$. As was mentioned earlier, it is difficult to obtain the exact variation of α in a flow with a wide range of Knudsen numbers in advance. Karniadakis *et al.*[4] suggested an averaged value, i.e., $\bar{\alpha}=2.2$, for nitrogen flow through a channel with $l/h=20$ and $\mathrm{Kn}_{\mathrm{out}}=0.2$. The main advantage of Eq. (18) over the one given by Eq. (21) is that it does not depend on any arbitrary constant and agrees quite accurately with the experiment. We highlight this point in Sec. III B.

B. Evaluating the derived IP-based slip coefficient model

After deriving analytical IP-based model expressions for both the volumetric and mass flow rates, we now consider their accuracies against other analytical solutions and available experimental data. Figure 6 shows the variation of the normalized volumetric flow rate with the Knudsen number. In this figure, Q_c is defined as the volumetric flow rate at the continuum limit. The volume flow rate of the current IP-based model, Eq. (17), is compared to those obtained from imposing different slip boundary conditions including the first-order Maxwell,[4] the second-order kinetic-theory, Eq. (1), the Aubert and Colin model,[6] the Hadjiconstantinou model,[34] and the Beskok model.[7] The slip coefficients (C_1

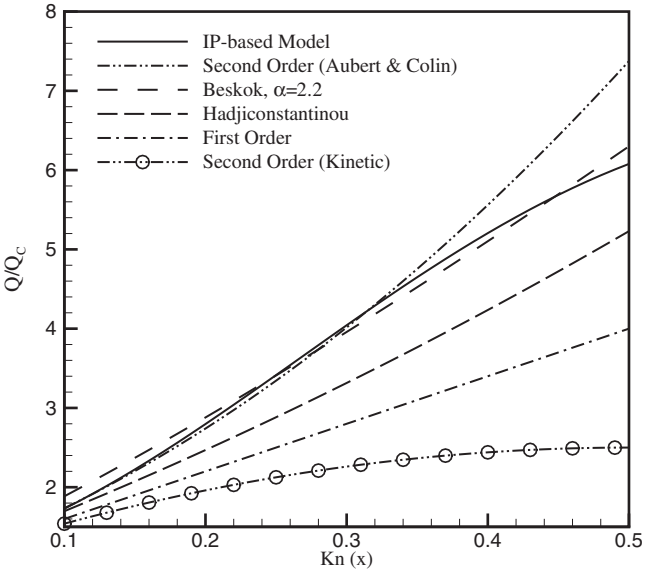

FIG. 6. Variation of current IP volumetric flow rate with Knudsen number and comparisons with different analytical models including the Aubert and Colin model (Ref. 6), Beskok and Karniadakis (Ref. 7), Hadjiconstantinou (Ref. 34), and the first- and second-order boundary conditions (Ref. 4).

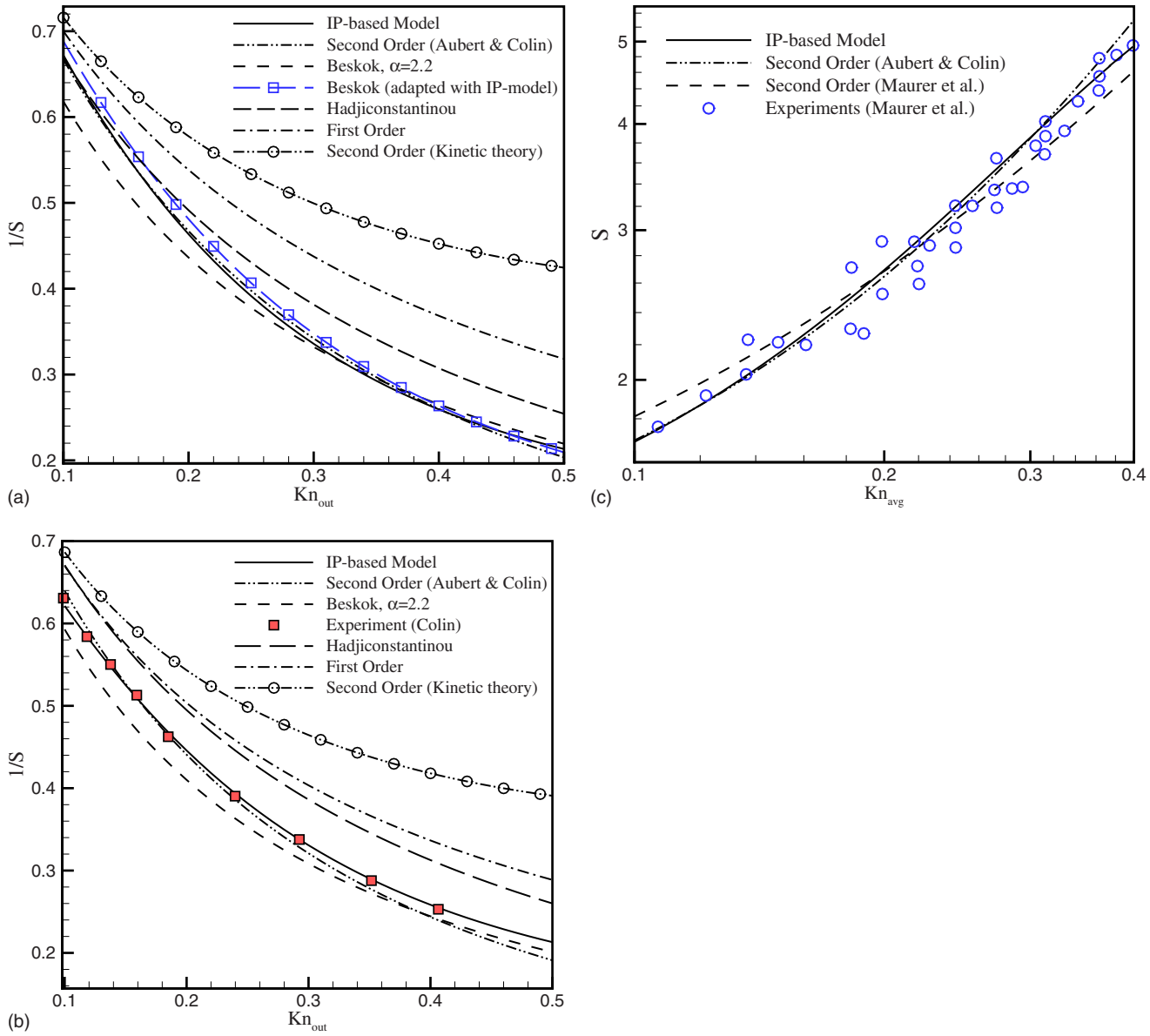

FIG. 7. (Color online) Variation of the IP-based slip coefficient expression [Eq. (18)] with the Knudsen number and comparison with different analytical models including those of Aubert and Colin (Ref. 6), Maurer *et al.* (Ref. 36), the first- and second-order boundary conditions (Ref. 4), and experimental data (Refs. 35 and 36). (a) $\Pi=2$, $\sigma_v=1$; (b) $\Pi=1.8$, $\sigma_v=0.93$; (c) $\Pi=2$, $\sigma_v=1$.

and C_2) for these boundary conditions are summarized in Table I. As can be seen, the second-order kinetic-theory model, Eq. (1), without implementing suitable viscosity modification performs the worst compared to the other models. However, this is to be expected because it has been derived in a manner to predict only a correct slip velocity at the wall. Compared to the Aubert and Colin model, the current IP-based slip coefficient model performs well. As stated previously, the second-order model of Aubert and Colin is accurate only for $\mathrm{Kn}<0.25$. Our IP-based model not only yields the same accuracy in this range but also agrees well with the trend predicted by the Beskok formula for the rest of the range. Compared to the Aubert and Colin model and our IP-based model, the Beskok formula yields poor results for $\mathrm{Kn}<0.2$ due to using a mean value of $\bar{\alpha}=2.2$ for the whole Knudsen number range. Interestingly, the current IP-based model, Aubert and Colin model, and Beskok model exhibit different curvatures, which are due to employing different types of slip-viscosity combinations.

In the next attempt, we compare the results of our mass flow rate modeling, Eq. (18), with those derived from other slip models, see Fig. 7. Figure 7(a) shows the variation of inverse slip coefficient with Knudsen number at the outlet of channel considering $\Pi=2$ and $\sigma_v=1$. The inverse slip is taken from Eqs. (18)–(21) using appropriate slip coefficients, as provided in Table I. Very similar to Fig. 6, it is observed that the IP-based model shows the closest agreement with the Aubert and Colin model. The Beskok solution with a constant α overestimates the slip for $\mathrm{Kn}<0.3$. We further study the performance of the Beskok slip model after incorporating it with the IP-based viscosity coefficient model. The slip coefficient obtained after this incorporation approaches the

Aubert and Colin slip model. Other models, such as the first-order and the original second-order models show considerable deviation from the Aubert and Colin model and the current IP-based model.

Further to this, we compare our results with the experiment,[35] which provides the slip variation for $\Pi=1.8$ and $\sigma=0.93$. As may be seen in Fig. 7(b), the results of current IP-based viscosity coefficient model agree well with the experimental data. This is where the analytical formula of Aubert and Colin departs from the given data for $\mathrm{Kn}>0.25$. The Beskok model does not match the experimental data at all. This may be due to setting a constant $b=-1$ in Eq. (3), and/or considering the suggested mean value for α, which may be derived for a full accommodation coefficient.[4] The figure also shows minimal sensitivity of the IP-based viscosity coefficient to the momentum accommodation coefficient. As stated previously, the IP simulations were performed for full momentum accommodation; however, it is currently applied for a lower accommodation value with no apparent adverse effect.

Figure 7(c) shows the variation of slip coefficient with the average Knudsen number, which is defined as $\mathrm{Kn}_{\mathrm{avg}}=(\mathrm{Kn}_{\mathrm{in}}+\mathrm{Kn}_{\mathrm{out}})/2$, for the current IP-based model, the Aubert and Colin formula, and the experimental data and empirical formula of Maurer *et al.*,[36] considering $\Pi=2$ and $\sigma_v=1$. The Maurer empirical expression for slip coefficient is given by

$$S=1+6A_1\ \mathrm{Kn}_{\mathrm{avg}}+12A_2\ \mathrm{Kn}_{\mathrm{avg}}^2, \tag{22}$$

where A_1 and A_2 are two constants, which depend on the gas molecule type. They are $A_1=1.3$ and $A_2=0.26$ for nitrogen flow. The results show that the current model agrees well with the scattered experimental data in the entire range of the investigated Knudsen numbers. This achievement can be attributed to developing a correct IP-based viscosity coefficient and benefiting from suitable accuracy of the second-order kinetic-based boundary condition. The range of accuracy for the current IP-based model formula is quite comparable with that of the kinetic-based regularized 13 moments (R13) equations as well. The R13 equations are a macroscopic set of transport equations of the third order in terms of the Knudsen number. As is demonstrated in Refs. 37 and 38, the full R13 equations result in an accurate solution for volume flow rate for $\mathrm{Kn}<0.5$. Similarly, the current IP-based model also predicts mass flow rate quite reliably for $0.1<\mathrm{Kn}<0.5$.

C. Effect of pressure ratio

The analytical expressions derived for the mass flow rate depends on both the Knudsen number and pressure ratio parameters, see Eq. (18). In Sec. III B, we demonstrated the variation of slip coefficient with outlet Knudsen number using different slip velocity models. At this stage, we further wish to consider the impact of pressure ratio variations on the slip coefficient expression. The current IP-based slip coefficient model is compared to different analytical models and experimental measurements for $\mathrm{Kn}_{\mathrm{out}}=0.15$, see Fig. 8(a). The experimental data have been taken from Ref. 35

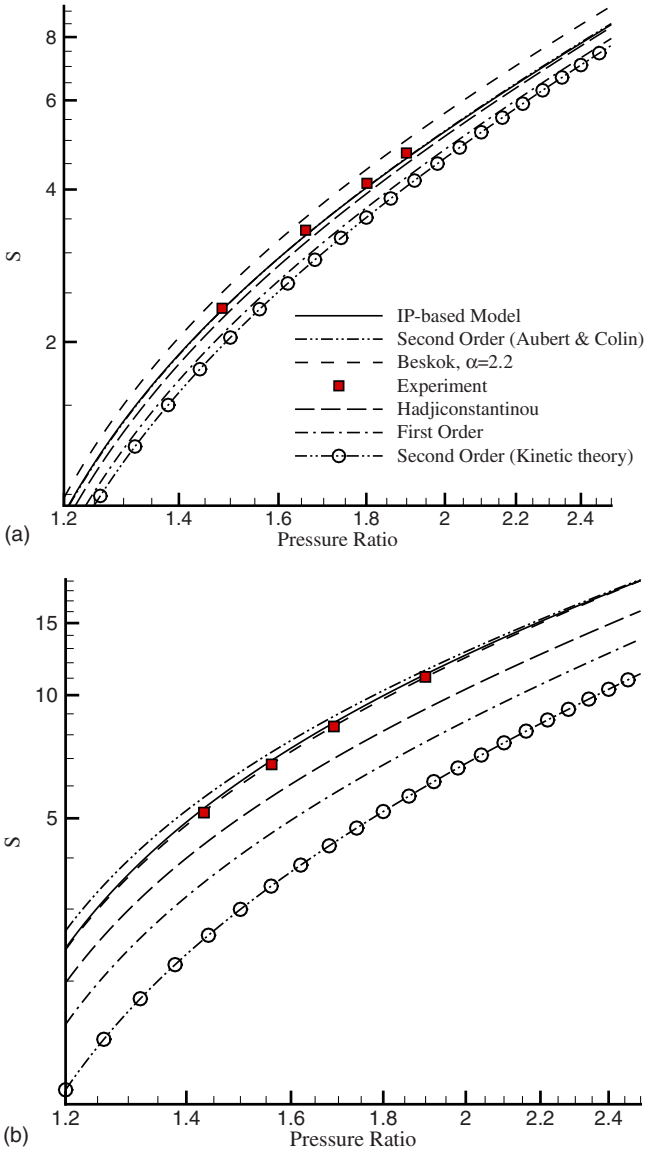

FIG. 8. (Color online) Variation of current IP-based slip coefficient expression with pressure ratio and comparison with those of other analytical models [including those of Aubert and Colin (Ref. 6), Beskok and Karniadakis (Ref. 7), Hadjiconstantinou (Ref. 34), and the first- and second-order boundary conditions (Ref. 4)], and experimental data (Ref. 35). (a) $\mathrm{Kn}_{\mathrm{out}}=0.15$; (b) $\mathrm{Kn}_{\mathrm{out}}=0.47$.

and have been suitably normalized. The results of our IP-based slip coefficient agree reasonably well with those of the Aubert and Colin formula and experimental data. This is where the Beskok model (with $\alpha=2.2$) overpredicts the slip value. The figure indicates that our IP-based analytical expression, which was originally derived for a pressure ratio of 2, can be reliably used for a wider range of pressure ratios without degrading its accuracy.

Increasing the outlet Knudsen number to 0.47, the IP-based model results in accurate solutions comparable with the experimental data and the solution resulting from the Beskok model, see Fig. 8(b). The agreement of the IP-based model with the Beskok formula is mainly due to the selection of an appropriate value for α, i.e., $\alpha=2.2$, which is suitable for the current Knudsen number. Figure 8(b) also indi-

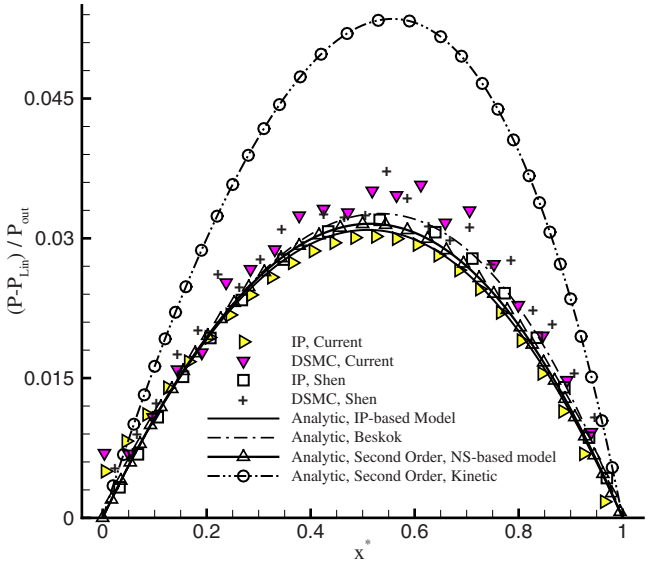

FIG. 9. (Color online) Deviation of current analytical IP axial pressure distribution from the linear one (P_{Lin}) and comparison with those of the molecular-based solutions [current DSMC-IP solution, and DSMC-IP solution of Shen (Ref. 39)], analytical solutions [including the NS-based model, the Beskok model (Ref. 7), and the second-order boundary condition (Ref. 4)], $Kn_{out}=0.194$.

cates that the Aubert and Colin model shows a slight overprediction in the entire range of study while the other models, such as the first-order,[4] second-order,[4] and Hadjiconstantinou[34] models, underpredict the slip coefficient in this range.

D. Axial pressure distribution

Up to this point, we have evaluated the accuracy of our IP-based viscosity coefficient model in the prediction of mass flow rate in a microchannel flow. Another important parameter which must be carefully studied is the axial pressure distribution in the channel. The axial pressure distribution can be obtained via the conservation of mass flow rate through the channel. This results in a nonlinear equation for the axial pressure distribution, which can be solved iteratively. Figure 9 shows the deviation of the current IP-based model axial pressure from the linear axial pressure distribution. It is compared to those of the other analytical models, including the NS-based model, Eq. (14), the Beskok model,[7] and the second-order kinetic theory,[4] as well as our DSMC and IP solutions and the DSMC and IP solutions of Shen.[39] The distance is normalized by the channel length ($x^*=x/l$). The current IP-based analytical model, our DSMC and IP solutions, and the DSMC and IP solutions of Shen[39] showed a maximum deviation of approximately 0.03 at the midchannel. This consistency confirms the accuracy of our developed IP-based viscosity coefficient model. It is observed that the second-order kinetic model greatly overpredicts the pressure deviations and shows a maximum deviation of about 0.053 at the midchannel. The Aubert and Colin and Beskok models (using $\alpha=6$, which is higher than the suggested mean value of 2.2) also show good agreement with the DSMC-IP solutions. It can be concluded that the selection of a correct viscosity coefficient can also result in accurate pressure distribution.

IV. CONCLUSION

In order to extend the applicability of the NS equations beyond the slip flow regime and into the early transition regime in the two-dimensional (2D) channel flow regime, we implemented the wall shear stress distribution derived from IP simulations and formulated an analytical expression for the variation of viscosity coefficient in terms of the Knudsen number. It has been shown that the kinetic-theory-based slip boundary condition accurately predicts the velocity profile in the early transition regime. However, it fails to predict the mass flow rate accurately without the incorporation of rarefaction effects. Alternatively, through the use of IP results, we derived a modified viscosity coefficient expression in order to enable the NS equations to predict not only a suitable velocity profile but also the correct mass flow rate magnitude together with the streamwise pressure distribution in the 2D micro- and nanochannel flow treatments. Prior to deriving the viscosity coefficient, we compared the mass flow rate, wall shear stress, and velocity distribution from IP solution with those of DSMC and LB equations. It was shown that IP solution predicts consistent results. Assuming a linear relation between the shear stress and the velocity gradient and accounting for the limited accuracy of the kinetic-theory-based slip model up to $Kn<0.5$, the current IP-based viscosity coefficient model may be considered to be limited to the same range of Knudsen numbers. Compared to experimental data and analytical models, the current IP-based model accurately predicts the mass flow rate for the entire range of study, $0.1<Kn<0.5$, and also over a wide range of pressure ratios. In comparison with previous models such as the Beskok model, a key advantage of the current model is that it does not depend on any adjustable parameter, which must normally be determined after solving the actual flow field.

ACKNOWLEDGMENTS

The authors would like to thank Dr. Shidvash Vakilipour (Sharif University of Technology, Iran) for suggestions to extend the current work and Dr. Tom Scanlon (University of Strathclyde, U.K.) for reading of the manuscript. The authors acknowledge the financial support received from Sharif University of Technology, Iran.

[1] S. G. Kandlikar, S. Garimella, D. Li, S. Colin, and M. R. King, *Heat Transfer and Fluid Flow in Minichannels and Microchannels* (Elsevier, London, 2006).
[2] G. A. Bird, *Molecular Gas Dynamics and the Direct Simulation of Gas Flows* (Clarendon, Oxford, 1994).
[3] J. Fan and C. Shen, "Statistical simulation of low-speed unidirectional flows in transition regime," in *Rarefied Gas Dynamics, 2*, edited by R. Brun, R. Campargue, R. Gatignol, and J. C. Lengrand (Cepadus-Editions, Toulouse, 1999).
[4] G. E. Karniadakis, A. Beskok, and N. Aluru, *Microflows and Nanoflows: Fundamentals and Simulation* (Springer-Verlag, New York, 2005).
[5] R. W. Barber and D. R. Emerson, "Challenges in modeling gas-phase flow in microchannels: From slip to transition," Heat Transfer Eng. **27**, 3 (2006).
[6] C. Aubert and S. Colin, "High-order boundary conditions for gaseous

flows in rectangular microducts," Microscale Thermophys. Eng. **5**, 41 (2001).
[7]A. Beskok and G. E. Karniadakis, "A model for flows in channels, pipes, and ducts at micro and nano scales," Microscale Thermophys. Eng. **3**, 43 (1999).
[8]S. Colin, P. Lalonde, and R. Caen, "Validation of a second-order slip flow model in rectangular microchannels," Heat Transfer Eng. **25**, 23 (2004).
[9]M. Darbandi and S. Vakilipour, "Developing consistent inlet boundary conditions to study the entrance zone in microchannels," J. Thermophys. Heat Transfer **21**, 596 (2007).
[10]M. Darbandi and S. Vakilipour, "Solution of thermally developing zone in short micro/nano scale channels," ASME J. Heat Transfer **131**, 044501 (2009).
[11]S. Vakilipour and M. Darbandi, "Advancement in numerical study of gas flow and heat transfer in microchannels," J. Thermophys. Heat Transfer **23**, 205 (2009).
[12]M. Darbandi and G. E. Schneider, "Performance of an analogy-based all-speed procedure without any explicit damping," Comput. Mech. **26**, 459 (2000).
[13]M. Darbandi and S. Vakilipour, "Developing implicit pressure-weighted upwinding scheme to calculate steady and unsteady flows on unstructured grids," Int. J. Numer. Methods Fluids **56**, 115 (2008).
[14]M. Darbandi, E. Roohi, and V. Mokarizadeh, "Conceptual linearization of Euler governing equations to solve high speed compressible flow using a pressure-based method," Numer. Methods Partial Differ. Equ. **24**, 583 (2008).
[15]N. Dongari, Ab. Agrawal, and Ag. Agrawal, "Analytical solution of gaseous slip flow in long microchannels," Int. J. Heat Mass Transfer **50**, 3411 (2007).
[16]N. Dongari, A. Sharma, and F. Durst, "Pressure-driven diffusive gas flows in micro-channels: From the Knudsen to the continuum regimes," Microfluid. Nanofluid. **6**, 679 (2009).
[17]T. Zhang, L. Jia, and Z. Wang, "Validation of Navier–Stokes equations for slip flow analysis within transition region," Int. J. Heat Mass Transfer **51**, 6323 (2008).
[18]M. Darbandi, S. Vakilipour, F. Rikhtegar, and G. E. Schneider, "Finite volume simulation of gaseous microflows using modified boundary conditions," AIAA Paper No. 2007-0934, 2007.
[19]M. Darbandi, F. Rikhtegar, and G. E. Schneider, "Simulation of rarefied micro to nano gas flows using improved slip flow models," AIAA Paper No. 2007-3991, 2007.
[20]D. A. Lockerby, J. M. Reese, and M. A. Gallis, "Capturing the Knudsen layer in continuum-fluid models of non equilibrium gas flows," AIAA J. **43**, 1391 (2005).
[21]L. O'Hare, T. J. Scanlon, D. R. Emerson, and J. M. Reese, "Evaluating constitutive scaling models for application to compressible microflows," Int. J. Heat Mass Transfer **51**, 1281 (2008).
[22]Y. Fang and W. W. Liou, "Computations of the flow and heat transfer in microdevices using DSMC with implicit boundary conditions," ASME J. Heat Transfer **124**, 338 (2002).
[23]M. Wang and Z. Li, "Simulations for gas flows in microgeometries using the direct simulation Monte Carlo method," Int. J. Heat Fluid Flow **25**, 975 (2004).
[24]E. Roohi, M. Darbandi, and V. Mirjalili, "DSMC solution of supersonic scale to choked subsonic flow in micro to nano channels," Proceedings of the Sixth International ASME Conference on Nanochannels, Microchannels and Minichannels, Germany, 2008, Paper No. ICNMM2008-62282.
[25]E. Roohi, M. Darbandi, and V. Mirjalili, "Direct simulation Monte Carlo solution of subsonic flow through micro-nano scale channels," J. Heat Transfer **131**, 092402 (2009).
[26]E. Roohi, M. Darbandi, and V. Mirjalili, "Study of gas flow in micronozzle using an unstructured DSMC method," The Seventh International ASME Conference on Nanochannels, Microchannels and Minichannels, South Korea, 2009, Paper No. ICNMM2009-82180.
[27]C. Cai, I. D. Boyd, J. Fan, and G. V. Candler, "Direct simulation methods for low-speed microchannel flows," J. Thermophys. Heat Transfer **14**, 368 (2000).
[28]J. Fan, I. D. Boyd, C. Cai, K. Hennighausen, and G. V. Candler, "Computation of rarefied flows around a NACA 0012 airfoil," AIAA J. **39**, 618 (2001).
[29]Q. Sun and I. D. Boyd, "A direct simulation method for subsonic micro-scale gas flows," J. Comput. Phys. **179**, 400 (2002).
[30]C. Shen, J. Fan, and C. Xie, "Statistical simulation of rarefied gas flows in micro-channels," J. Comput. Phys. **189**, 512 (2003).
[31]W. W. Liou and Y. Fang, *Microfluid Mechanics: Principles and Modeling* (McGraw-Hill, London, 2006).
[32]M. Ilgaz and M. C. Çelenligil, "DSMC simulations of low-density choked flow in parallel-plate channels," AIP Conf. Proc. **663**, 831 (2003).
[33]T. Ohwada, Y. Sone, and K. Aoki, "Numerical analysis of the Poiseuille and thermal transpiration flows between two parallel plates on the basis of the Boltzmann equation for hard sphere molecules," Phys. Fluids A **1**, 2042 (1989).
[34]N. G. Hadjiconstantinou, "Comment on Cercignani's second-order slip coefficient," Phys. Fluids **15**, 2352 (2003).
[35]S. Colin, "Rarefaction and compressibility effects on steady and transient gas flow in microchannels," Microfluid. Nanofluid. **1**, 268 (2005).
[36]J. Maurer, P. Tabelin, P. Joseph, and H. Willaime, "Second-order slip laws in microchannels for helium and nitrogen," Phys. Fluids **15**, 2613 (2003).
[37]H. Struchtrup and M. Torrilhon, "Higher-order effects in rarefied channel flows," Phys. Rev. E **78**, 046301 (2008).
[38]P. Taheri, M. Torrilhon, and H. Struchtrup, "Couette and Poiseuille microflows: Analytical solution for regulized 13-moment equations," Phys. Fluids **21**, 017102 (2009).
[39]C. Shen, *Rarefied Gas Dynamics: Fundamentals, Simulations and Micro Flows* (Springer-Verlag, Berlin, Heidelberg, 2005).